Sustainable Energy Technologies and Assessments 87 (2026) 104915

Contents lists available at ScienceDirect

Sustainable Energy Technologies and Assessments

journal homepage: www.elsevier.com/locate/seta

Silk Fibroin-Based bioanodes integrating *Bacillus subtilis* and Prussian blue for Rapidly activated and High-Performance microbial fuel cells☆

Pablo Rodríguez-Núñez [a], Sebastián Gavira-Aguilar [a], Silvia Mena [a], Aida Visús [a], Nuria Vigués [b], Jordi Mas [b], Salvador D. Aznar-Cervantes [c], Naroa Uria [d], Ignacio Moro [d], Antonio Solares [d], Sara Santiago [e], Xavier Muñoz-Berbel [a,*]

[a] Institute of Microelectronics of Barcelona (IMB-CNM, CSIC), Autonomous University of Barcelona Sphere, Cerdanyola del Vallès, Barcelona 08193, Spain
[b] Department of Genetics and Microbiology, Autonomous University of Barcelona, Cerdanyola del Vallès, Barcelona 08193, Spain
[c] Department of Biotechnology, Genomics and Plant Breeding, Murcian Institute of Agricultural and Environmental Research and Development (IMIDA), 30150 La Alberca, Murcia, Spain
[d] Arkyne Technologies SL (Bioo) ES-B90229261, Viladecans, 08840 Barcelona, Spain
[e] Department of Materials and Environmental Chemistry. Stockholm University, 106 91, Stockholm, Sweden

ARTICLE INFO

Keywords:
Soil-microbial fuel cells
Microbial bioanode
Silk fibroin immobilization
Prussian Blue mediator
Sustainable energy

ABSTRACT

Soil microbial fuel cells (sMFC) are promising bioelectrochemical systems that convert organic matter in soil into electricity via microbial metabolism. However, their practical deployment is hindered by low efficiency, limited scalability, and the long start-ups time required for biofilm formation. This study introduces a synergistic immobilization strategy that integrates both electrogenic bacteria and redox mediators directly onto the anode surface. *Bacillus subtilis*, a soil-dwelling electrogenic bacterium, was encapsulated within silk fibroin (SF) membranes using a one-step green chemical process that ensures high bacterial viability and strong adhesion to large-area carbon anodes (95 cm^2). Co-immobilization of Prussian blue (PB) within the SF matrix enhanced electron transfer between microorganisms and electrodes. The dual-functionalized bioanodes nearly doubled the maximum current output (2.5 mA vs. 1.5 mA), and reduced start-up time from 8 to 4 days. After one month, SF membranes remained structurally stable and supported active microbial colonization, confirming their durability and biocompatibility. These findings demonstrated that simultaneous immobilization of electrogenic bacteria and redox mediators accelerated biofilm activation and boosted energy generation, positioning SF as a scalable platform for sustainable, field-ready microbial bio-batteries.

Introduction

Microbial fuel cells (MFCs) are bio-electrochemical systems that exploit microbial metabolism to oxidize organic substrates and transfer electrons to an electrode under anaerobic conditions [1]. Beyond power generation, MFCs enable wastewater or soil remediation [2]. Their ability to utilize diverse organic wastes while operating at ambient temperature without pollutant emissions makes them promising for decentralized and sustainable energy production [3,4].

Despite these advantages, MFCs implementation is often limited by the slow and progressive formation of electroactive biofilms on the anode, which can take several weeks to achieve efficient electron transfer [5]. Preformed microbial bioanodes can reduce start-up times, but bacterial immobilization remains challenging because many fabrication methods expose cells to dehydration, heat, radiation or chemicals that reduce viability [6].

Alginate hydrogels provide mild encapsulation conditions [7–9], reducing start-up times [10] and increasing current output [11]. However, alginate does not recover its hydrated state once dehydrated, leading to irreversible matrix shrinkage and bacterial death. This critical limitation, exacerbated by its low mechanical stability, makes alginate unsuitable for long-term operation, particularly in systems prone to periodic dehydration.

Silk fibroin (SF), derived from *Bombyx mori*, offers high mechanical

☆ This article is part of a special issue entitled: 'MEEP 2025' published in Sustainable Energy Technologies and Assessments.

* Corresponding author at: Institute of Microelectronics of Barcelona (IMB-CNM, CSIC), Autonomous University of Barcelona Sphere, Cerdanyola del Vallès, 08193 Barcelona, Spain.
E-mail address: xavier.munoz@imb-cnm.csic.es (X. Muñoz-Berbel).

https://doi.org/10.1016/j.seta.2026.104915
Received 16 December 2025; Received in revised form 9 February 2026; Accepted 2 March 2026

strength, biocompatibility and ability to stabilize biological components. SF self-assembles into β-sheet-rich domains that confer chemical and structural stability [12], and it has been used to immobilize enzymes [13–15], antibiotics [16], antibodies [14] and living cells [17,18], while preserving both bacterial [19] and enzymatic activity [20].

The formation of robust SF films requires controlled crystallization, which converts amorphous regions into β-sheet crystalline domains to enhance durability and reduce solubility [21]. However, conventional crystallization methods can damage cells through dehydration or oxidative stress [22].

Here, we introduce a one-step, biocompatible SF immobilization strategy that preserves the viability of the electrogenic bacterium Bacillus subtilis [23,24] and enables the co-immobilization of Prussian blue (PB), a redox mediator that enhances bacteria-electrode electron transfer in both solution-based [25–27] and solid-state systems [28,29]. The resulting dual-functional bioanode accelerates start-up and enhances current generation in MFCs, providing a scalable and robust approach for next-generation bioelectrochemical energy systems.

Methods

Chemicals and materials

Silk fibroin (SF, 7% w/v) was provided by IMIDA (Spain). Phosphate buffered saline (PBS; Fisher Scientific, USA), green chemical compound (GCC; Tokio Chemical Industry Co., Japan), Iron sulfate ($FeSO_4$, ≥99.0%; Panreac AppliChem, Spain), potassium ferricyanide ($K_3[Fe(CN)_6]$, ≥99.0%; Panreac AppliChem, Spain), D-(+)-glucose (≥99.5%; Sigma-Aldrich, USA), hydrochloric acid (HCl, 36%; Sigma-Aldrich, USA) and potassium chloride (KCl, ≥99.0%; Sigma-Aldrich, USA) were of chemical grade and used as received. Aqueous solutions were prepared using de-ionized water (18 MΩ/cm).

Custom-made electrodes (Fig. S1A) were screen printed using conductive inks: Ag (LOCTITE ECI 1010, Cyclops Synergies, Spain), Prussian blue-graphite (SunChemical C2070424P2, IMCD, Spain), carbon-graphite (SunChemical C2030519P4, IMCD, Spain), and Ag/AgCl (SunChemical C2130809D5, IMCD, Spain) inks on polyethylene terephthalate (PET) substrates (STS A.00-A.00, Cyclops Synergies, Spain) with pressure sensitive adhesive (PSA, ARcare® 8939, Adhesive Research, Ireland) used as isolating layer. Printing screens and squeegees were obtained from Paymer (Spain). Polymethyl methacrylate (PMMA) sheets (3 mm, Evonik Industries AG, Germany) were used for the electrochemical platform.

Bacterial cultures preparation

Bacillus subtilis NCTC 8236 was grown aerobically in Luria-Bertani (LB) broth for 18 h at 30°C in a shaker bath (120 rpm). For electrochemical studies, anaerobic cultures were prepared in minimal medium AB (MMAB) [30] supplemented with 0.2% glucose and incubated at 30°C under N_2 bubbling for 48 h. Cultures were centrifuged (Eppendorf 5804R, Germany) at 4000 rpm for 10 min and re-suspended in sterile distilled water. An optical density at 600 nm (OD_{600nm}, SmartspecTM Plus spectrophotometer, BioRad, USA) of 0.2 a.u. corresponded to 10^8 colony forming units per mL ($CFU{\cdot}mL^{-1}$), which verified by plate counting.

Electrochemical characterization of Bacillus subtilis

The electron transfer capacity of *Bacillus subtilis* was evaluated under aerobic (18 h culture in LB at 30°C) and anaerobic cultures (48 h culture in MMAB supplemented with 0.2% glucose at 30°C under continuous N_2 bubbling). PB-modified and unmodified carbon electrodes were incubated with bacterial suspensions for 24 h to promote biofilm formation (details in Fig. S1B), rinsed with PBS to remove planktonic cells, and analyzed by differential pulse voltammetry (DPV).

DPV was selected due to its high sensitivity for detecting low-abundance redox mediators and metabolic electron-transfer signals in living cells [31], resulting from the effective reduction of capacitive background currents and the enhances resolution of faradaic processes. These characteristics make DPV particularly suitable for complex biological matrices, where conventional voltammetric techniques may be strongly compromised by high background currents and matrix interferences [32].

Electrochemical measurements were performed using a μSTAT8000 multi-potentiostat (Dropsens, Spain) in 0.1 M KCl, employing a three-electrode configuration with an integrated Ag/AgCl pseudo-reference electrode. The potential window (−0.2 to + 1.0 V vs. Ag/AgCl) was carefully selected based on preliminary cyclic voltammetry experiments to encompass PB/PW redox transition [27] as well as other potential redox-active mediators involved in bacterial electron transfer [30] At the same time, this window avoided potential regions associated with oxygen reduction and water oxidation, thereby minimizing parasitic reaction and cell damage.

A slow scan rate (0.01 V/s) was employed to enhance sensitivity under diffusion-controlled conditions and to enable the detection of weak or kinetically slow redox processes associated with microbial electron transfer. This choice is consistent with previous experimental observations showing that biologically relevant redox signals from bacterial systems are often undetectable at higher scan rates but become resolvable under slow potential sweeps [30]. The step potential (2 mV), the pulse amplitude (10 mV) and the pulse duration (10 ms) were selected according to the recommendations of the manufacturer. Baseline DPV curves were recorded in 0.1 M KCl prior to bacterial incubation.

Bacterial immobilization and viability

Bacillus subtilis was immobilized in SF films (25 μm) by drop-casting a SF suspension (7% w/v SF) containing 5×10^8 $CFU{\cdot}mL^{-1}$ onto Petri dishes, followed by drying at 37°C for 5 h to induce crystallization. Bacterial viability was evaluated by (i) fluorescence microscopy using the Live/Dead BacLight™ kit (Fisher Chemical, USA) and (ii) colony counting on LB agar plates. SF films were prepared and handled under aseptic conditions, either in a laminar flow cabinet or in the vicinity of a Bunsen burner flame depending on the assay, to prevent contamination prior to bacterial immobilization. Autoclaving of the SF solution was avoided to preserve the structural and biological compatibility of the SF matrix.

For fluorescence microscopy, viability was assessed at three stages: (i) fresh culture (control), (ii) pre-crystallization (SF solution before drying) and (iii) post crystallization (after vacuum water annealing or GCC treatment). Films were stained for 15 min in the dark, where live and dead bacteria were labeled with SYTO 9 (green) and propidium iodide (PI; red), respectively. After washing with PBS to remove excess dye, samples were imaged using an Axio imager A1 fluorescence microscope (ZEISS, Germany) with excitation filters at 480 nm (SYTO 9) and 490 nm (PI). Images were acquired at 40 × magnification and analyzed using the ImageJ software using five representative images per sample. Fourier-transform infrared spectroscopy (FTIR; Bruker Invenio-S IR spectrometer, Germany) confirmed β-sheet formation through the characteristic 1622 cm^{-1} peak in the amide I region (Fig. S2).

For plate counting, SF films were prepared as described but without GCC to maintain water solubility. Films were dissolved in 2 mL sterile Milli-Q water, serially diluted, and plated on LB agar. Bacterial counting from the initial SF-bacteria suspension before drying was used as reference to calculate survival rates.

Bacterial proliferation in SF films

Bacterial proliferation within SF films was evaluated by monitoring optical density changes in crystalline SF films containing *Bacillus subtilis*,

which placed on solid LB agar and incubated at 30°C for 48 h. In this configuration, bacterial growth relied on nutrients diffusion from the agar into the SF matrix. After incubation, the films were transferred to liquid LB medium to assess viability of encapsulated bacteria, their ability to proliferate and migrate out of the SF matrix.

Bioanode fabrication

Bioanodes were fabricated by using a novel GCC-mediated crystallization protocol (patent pending), as illustrated in Fig. 3S. Briefly, a 7% (w/v) SF solution was supplemented with 20% (w/v) GCC and the PB precursors $FeSO_4$ (450 mM) and $K_3[Fe(CN)_6$ (600 mM), followed by stirring until a homogeneous blue coloration appeared, indicating complete PB formation. The bacterial pellet obtained from 0.5 L of *Bacillus subtilis* culture growth overnight in LB under aerobic conditions was resuspended in 120 mL of the SF/PB solution. The suspension pH was adjusted to 7.0 using 0.1 M HCl to prevent PB degradation. Then, 10 mL of the SF/PB/*Bacillus subtilis* suspension was drop-cast onto a 95 cm^2 activated carbon felt electrode (BGF-1, CM Carbon, China) and evenly spread to ensure uniform film formation. The electrodes were dried at 37°C for 5 h to induce SF crystallization and stored at 4°C until use.

Soil MFCs (sMFCs) production and validation

Bioanodes (SF-PB-BS) and control electrodes (unmodified, SF, SF-PB, SF-BS) were assembled into 3D-printed polylactic acid (PLA) cylindrical reactors (11 cm diameter × 10.5 cm height). The reactors were equipped with activated carbon felt cathodes (95 cm^2, 3 mm thick) and titanium wire connectors. The anode and cathode were separated by an 8 cm gap, fully occupied by the horticultural soil substrate.

Three independent reactors were assembled for each of the five anodic treatments. Each reactor was filled with 500 g of horticultural soil supplemented with 1% (w/w) 5–5–5 NPK biochar and hydrated with 450 mL of water.

The sMFCs were operated at 25°C under automated irrigation (11 s every 12 h) and monitored using two custom Arduino-based systems: automatic open circuit potential (AOCP) and automatic linear sweep voltammetry (ALSV). Initially, OCP was recorded in real time with the AOCP device for one week to allow system stabilization. Subsequently, reactors were connected to the ALSV systems, which operated as passive circuits utilizing the energy generated by the sMFC itself to perform voltage sweeps directly on the sMFC. This functionality was achieved through the controlled charging of a supercapacitor, while monitoring the voltage drops across a serial resistor to determine the charging current. A programmable switch regulated both the charge level of the supercapacitor and the voltage applied to the sMFC, enabling precise control of the electrochemical conditions.

The ALSV performed continuous forward and reverse voltage sweeps (from OCP to 0 mV and back) at a scan rate of 0.1075 $mV{\cdot}s^{-1}$, generating current–voltage (I-V) curves every 2 h. Power (P) produced by each sMFC was calculated using Ohḿs law ($P = V{\cdot}I$). Data obtained from I to V and power curves were processed to calculate the average and standard deviation values of triplicates on each time point. Four parameters were evaluated: maximum power, maximum current, open circuit voltage and accumulated energy.

Post-operation analysis

After one month of operation, anodes were analyzed by scanning electron microscopy (SEM; EVO MA10, ZEISS, Germany) and the PrestoBlue™ assay (Thermo Fisher Scientific, USA) to assess their structural integrity and metabolic activity. Microbial community analysis of the anode samples (n = 15, triplicates of C, SF, SF-BS, SF-PB, SF-PB-BS) was also conducted to evaluate how bacterial colonization influence bioanode performance and sMFC power output.

SEM images were acquired at a working distance of 4–6 mm, accelerating voltage (EHT) of 8 kV, and magnifications ranging from 2kX to 10kX.

In the PrestoBlue™ assay, the reduction of the resazurin reagent was quantified by fluorescence ($\lambda_{excitation}$ = 550 nm, $\lambda_{emission}$ = 600 nm) using a Varioskan Flash microplate reader (Thermo Fisher Scientific, USA).

Microbial communities were characterized by 16S rRNA sequencing (Novogene GmbH, Germany). Briefly, DNA was extracted using the Tiangen Magnetic Soil and Stool Kit (Tiangen Biotech, China), quantified with an Agilent 5400 Fragment Analyzer (Agilent Technologies, USA), and amplified using the 515F–806R primer pair targeting the 16SV3-V4 region (30 PCR cycles). Amplicons were purified with magnetic beads, indexed, and sequenced on Illumina platforms. Paired-end reads were processed using FLASH (V1.2. 1 1, https://ccb.jhu.edu/software/FLASH/) [33] to merge overlapping sequences, and fastp (Version 0.23.1) [34] to filter raw tags and generate high-quality Clean Tags. Chimera sequences were identified and removed using the VSEARCH package (V2.16.0, https://github.com/torognes/vsearch) [35]. Taxonomic annotation was performed using the Silva Database and QIIME2 software after normalization of the absolute abundances. Alpha diversity was computed using Shannon and Chao1 indices in QIIME2 to assess community diversity, richness, and evenness. Non-metric multidimensional scaling (NMDS) and additional community structure analyses were performed using the vegan package [36] in R [37].

Results and discussion

Direct and PB-mediated electron transfer of Bacillus subtilis

DPV was used to evaluate electron transfer processes of *Bacillus subtilis* on carbon and PB-modified electrodes under aerobic and anaerobic conditions (Fig. 1A). Prior to bacterial colonization, both electrode types exhibited stable and reproducible baselines, with PB electrodes displaying a characteristic oxidation peak at ~ 0.15 V (vs. Ag/AgCl) (Fig. 1Bi), corresponding to the oxidation of residual Prussian white (PW) to PB [26].

After *Bacillus* incubation, this peak increased markedly under both anaerobic (Fig. 1Bii) and aerobic (Fig. 1Biii) conditions, indicating metabolic reduction of PB by *Bacillus subtilis*. The stronger response observed under aerobic conditions is consistent with higher metabolic activity supported by oxygen respiration [27]. Under anaerobic conditions, an additional peak emerged at 0.5 V (vs.Ag/AgCl) on both PB-modified and unmodified electrodes (Fig. 1Bii), suggesting activation of direct or endogenous mediator-based electron-transfer pathways, as previously reported for bacterial electrochemical systems [38].

The use of low scan-rate DPV enabled resolution of these biologically relevant redox features, which are often undetectable at higher scan rates due to overlapping of capacitive currents and slow electron-transfer kinetics. These results confirmed that *Bacillus subtilis* can transfer electrons through direct and PB-mediated mechanisms, depending on oxygen availability, but the incorporation of PB significantly enhances current generation, validating its role as an effective mediator of metabolic electrons.

Bacterial viability and proliferation studies

Bacterial viability during SF film fabrication was evaluated at key stages using a Live/Dead fluorescence assay (Fig. 2A). Live/Dead staining was performed immediately after completion of the crystallization process, corresponding to the initial time point (t = 0h) of the proliferation assays, in order to assess bacterial survival during immobilization and film formation.

Bacillus subtilis incorporated into the SF solution before film casting exhibited a viability of 70 ± 8% (Fig. 2Aii), not significantly different from control cultures (73 ± 5%; Fig. 2Ai), confirming that exposure to

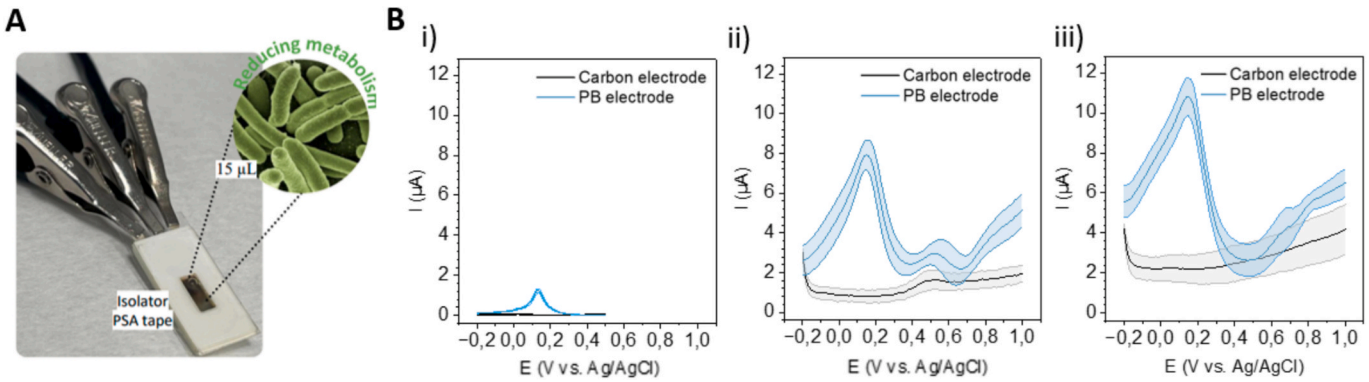

Fig. 1. DPV analysis of carbon and PB electrodes. (A) Electrodes connected to the potentiostat, with biofilm formed on the electrode surface. PSA tape was used to confine a 15 µL analyte suspension, ensuring consistent measurements. (B) Voltammograms of electrodes before bacterial colonization (i) and after biofilm formation by *Bacillus subtilis* under anaerobic (ii) anaerobic conditions (iii) are shown. Data represent mean ± standard deviation (n = 4).

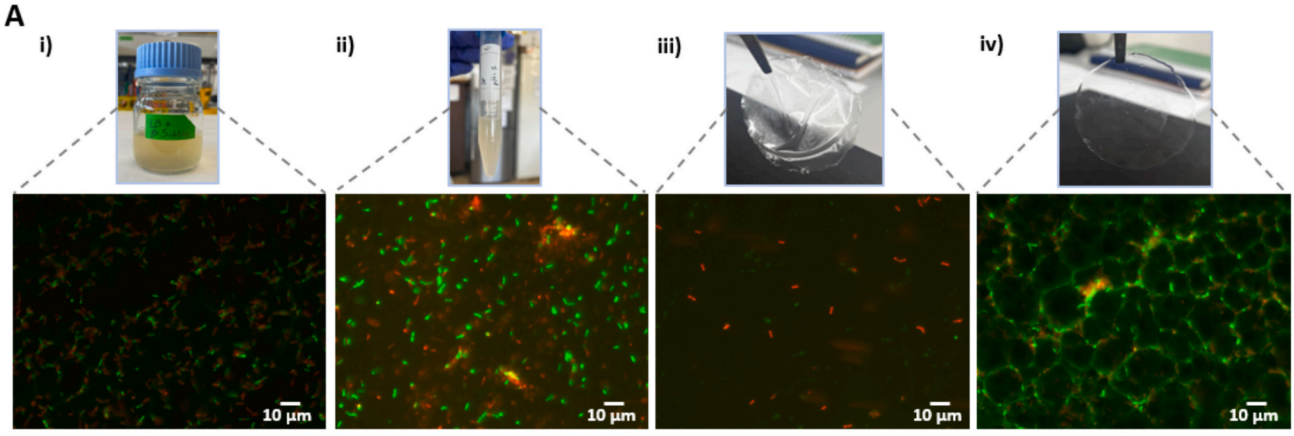

B

SF solution (Time zero)	Dried film (After 5h at 37°C)		Survival rate (%) (UFC $_{5h\ film}$ / UFC $_{Silk\ solution}$)
UFC/ml		UFC/cm²	
$7.7 \pm 3 \cdot 10^7$	$5.7 \pm 2 \cdot 10^7$	$1.8 \pm 0.5 \cdot 10^7$	**70.5 ± 3.6**

Fig. 2. *Bacillus subtilis* viability analysis during crystallization process. (A) Live/Dead Fluorescence microscopy images of *Bacillus subtilis* under different conditions: (i) Control overnight culture of *Bacillus subtilis* in LB medium, (ii) SF solution doped with *Bacillus subtilis* at time 0, (iii) SF film crystallized by the conventional vacuum protocol (5-hour drying at 37°C followed by 5 h under vacuum), showing a higher ratio of dead cells, and (iv) SF film crystallized by the GCC-mediated protocol (single 5-hour drying at 37°C), showing fewer dead cells compared to the conventional method. Scale bars: 10 µm. (B) Quantitative assessment of *Bacillus subtilis* survival following immobilization in SF films. Data represent mean ± standard deviation (n = 3).

the SF solution did not compromise bacterial survival [6]. Conventional two-step vacuum annealing (5 h drying + 5h water annealing at 37°C) caused a marked loss of viability (5%; Fig. 2Aiii), attributed to severe dehydration and structural cell damage under vacuum conditions. In contrast, the GCC-mediated single-step crystallization process (5 h drying at 37°C) retained 50–60% viability (Fig. 2Aiv), demonstrating that this milder process better preserved bacterial integrity.

As SF films exhibit strong green autofluorescence [39], viability was further verified by plate counting. SF-*Bacillus subtilis* films were dissolved in sterile water, serially diluted and plated on LB agar. The resulting CFUs, compared with the initial suspension before crystallization, exhibited 70 ± 4% survival, confirming that GCC-mediated protocol maintains high bacterial viability (Fig. 2B).

The ability of *Bacillus subtilis* to proliferate within the SF film was assessed to confirm metabolic activity relevant to energy generation in sMFC. Freshly prepared SF film containing *Bacillus subtilis* appeared transparent at time 0, indicating a low bacterial load. During incubation on LB-agar plates, the films progressively became opaque and whitish (Fig. 3A), whereas control SF films without bacteria remained transparent throughout the experiment. Although changes in opacity are not selective indicators of bacterial growth, this behavior was consistent with bacterial proliferation within the SF matrix and suggests that nutrients diffused from the agar into the SF film, sustaining microbial growth.

Upon prolonged incubation, limited colony formation was observed outside the SF films, mainly at the film edges. This observation indicates that bacterial retention within the SF matrix is predominant, while partial bacterial dispersal may occur over time. To further evaluate this behavior, SF films containing bacteria and non-doped SF films were transferred to liquid LB medium (Fig. 3B). LB medium without films was also included as negative control. After overnight incubation at 30°C, the medium containing bacteria-doped SF film exhibited visible turbidity, whereas both the medium containing non-doped SF film and the medium alone remained clear. While turbidity is a non-specific indicator, the inclusion of these controls excludes film degradation or medium-related effects and is consistent with bacterial release followed by proliferation in the liquid medium.

These observations demonstrate that SF matrices support bacterial

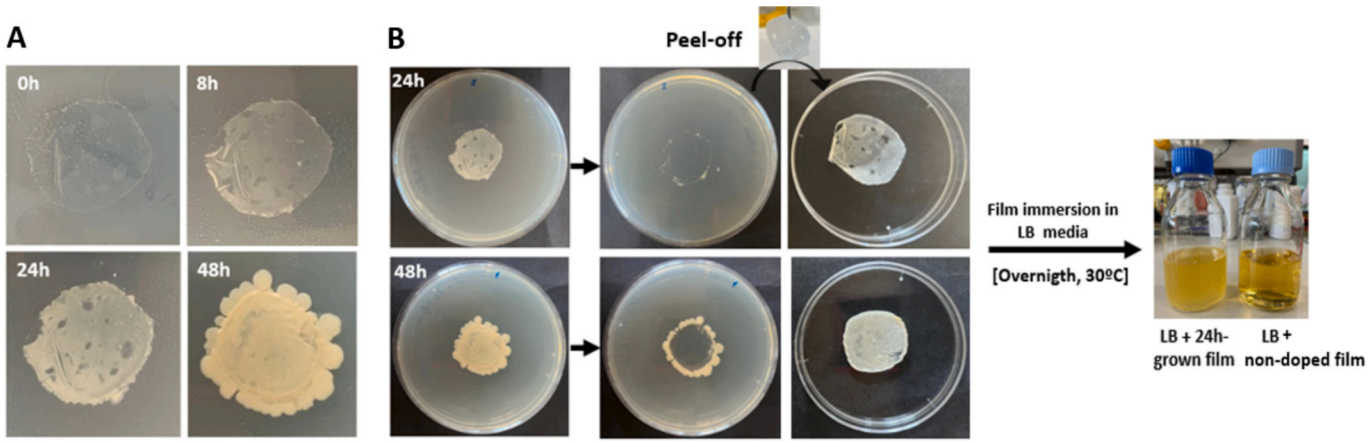

Fig. 3. Bacterial proliferation and release studies. (A) Time-lapse images of SF films containing *Bacillus subtilis* incubated on LB-agar at 0, 8, 24, and 48 h, showing increased opacity consistent with bacterial growth within the SF matrix. (B) After incubation, films were transferred to liquid LB medium. Increased turbidity after 24 h incubation at 30°C, observed only for bacteria-doped SF films and not for control films without bacteria or medium alone, is consistent with partial bacterial release and proliferation, although turbidity itself is non-specific.

survival, regrowth and limited dispersal, features that are favourable for effective bioanode colonization.

sMFC performance

The performance of sMFCs incorporating different bioanode configurations (raw carbon felt used as control, SF, SF-BS, SF-PB and SF-PB-BS) was monitored over one month by evaluating voltage, current, power and accumulated energy. The assembled sMFC prototype with the Arduino-based data acquisition system are shown in Fig. 4A.

OCP profiles over 40 days are presented in Fig. 4Bi. Control cells exhibited a lower initial voltage (100 mV) compared to modified electrodes (400 mV), likely due to the lower moisture content of untreated carbon felt electrodes relative to modified electrodes, which exposed to aqueous processing steps that improved hydration and ion conductivity. Anode-specific I-V curves obtained at the time of assembly (Fig. S4A) further support this interpretation, showing that the reduced OCP and current observed in control systems originate primarily from limitations

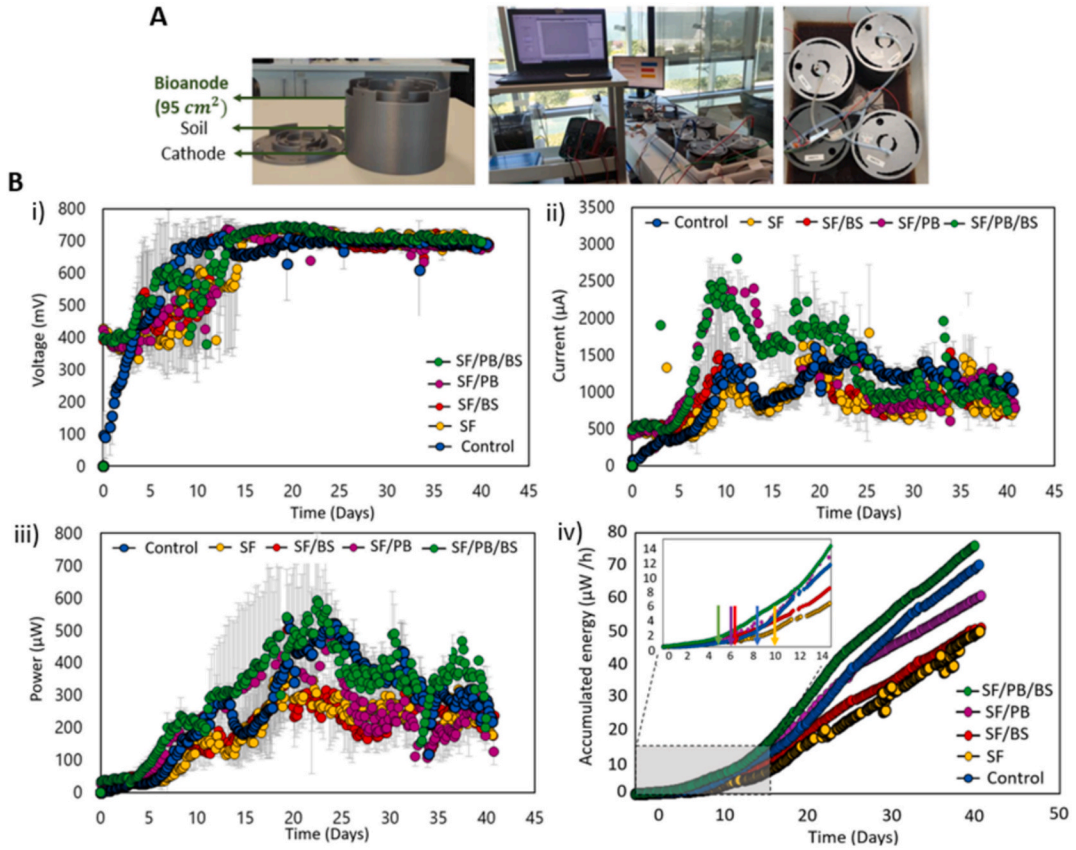

Fig. 4. Performance of different sMFC configurations over 40 days. (A) Prototype sMFC and Arduino-based monitoring system (BIOO). (B)(i) Voltage, (ii) current output, (iii) power and (iv) accumulated energy over time for control, SF, SF-BS, SF-PB and SF-PB-BS bioanodes. Points present average and standard deviation (n = 3) summarizing continuous measurements into single values every two hours.

at the non-functionalized anodes.

As operation progressed, all sMFCs showed gradual increases in OCP, attributed to the establishment of anaerobic conditions and biofilm development [40]. Among the different configurations, SF-PB-BS displayed the fastest OCP increase, reaching the highest value on day 19 (747 ± 8 mV). This behavior is consistent with the redox-mediating capacity of PB, which facilitates electron transfer and accelerates stabilization of anode potential by reducing charge-transfer resistance [41,42]. Correspondingly, I-V curves obtained on day 19 (Fig. S4B) show that the enhanced performance of SF-PB and SF-PB-BS systems is associated with reduced cathodic polarization, an effect previously linked to anodes capable of reaching more negative potentials at early stages of operation [40], as observed in these configurations (Fig. S4B).

Current generation trends (Fig. 4Bii) further confirmed PB contribution. sMFCs containing PB (SF-PB and SF-PB-BS) achieved the highest current outputs in the first three weeks, reaching 2.5 mA on day 10, approximately 68% higher than other configurations. In contrast, controls, SF and SF-BS systems exhibited comparable lower currents, highlighting the role of PB as an efficient redox mediator enhancing electron-transfer efficiency during early operations.

Power output evolution (Fig. 4Biii) followed similar trends. SF-PB-BS systems showed the most rapid power increase, reaching a maximum average power of 593 μW on day 22, followed by SF-PB. Control systems exhibited delayed power development but eventually approached comparable maximum values, while SF and SF-BS systems remained lower (around 300 μW). This behavior suggests that direct electron transfer between bacteria and exposed carbon fibers can partially compensate for the absence of mediators in uncoated electrodes, whereas silk-coated electrodes without PB may introduce diffusional and electrical barriers, reducing conductivity and power generation. Notably, between days 22 to day 40, the SF-PB-BS systems maintained superior performance relative to SF-PB, highlighting the positive effect of initial *Bacillus subtilis* immobilization on promoting bacterial recruitment and early biofilm formation.

Bioanode modification also significantly reduced the start-up time (Fig. 4Biv). SF-PB-BS systems initiated power generation by day 4, compared to 8–9 days for control systems. SF-PB and SF-BS electrodes also shortened start-up time to approximately 6 days, probably due to enhanced bacterial attachment mediated by the silk coating, although their total accumulated energy output remained below that of controls. This reduced performance of SF-PB and SF-BS may arise from limitations in nutrient and charge transfer diffusion within the thicker silk-based biofilms at later stages.

Overall, these results demonstrate that the combined use of silk fibroin, PB and *Bacillus subtilis* produces a highly effective bioanode that accelerates start-up, supports electrogenic biofilms development and facilitates efficient electron transfer, particularly during the early and intermediate phases of sMFC systems operation. Although the absolute power output of the sMFC is in the μW range, the obtained power densities are comparable to those reported for state-of-the-art soil MFCs [40], and are sufficient for low-power applications such as environmental sensors and IoT devices, when coupled with appropriate energy management systems [43].

Post-operation characterization of biofunctionalized electrodes

To evaluate the long-term stability, microbial colonization and electrogenic potential of the biofunctionalized anodes, a comprehensive post-operational analysis was conducted following one month of continuous operation. This analysis integrated structural assessment by SEM, metabolic activity measurements with resazurin, and 16S rRNA amplicon sequencing to elucidate how the electrode modifications influenced biofilm architecture, bioanode composition and the overall sMFC functionality.

SEM imaging revealed that SF-BS-PB electrodes maintained excellent structural integrity throughout operation (Fig. 5Aiii). The SF membrane persisted as a cohesive and continuous layer enveloping the carbon felt fibers, keeping the morphology observed immediately after fabrication (Fig. 5Ai). At higher magnifications, immobilized *Bacillus subtilis* cells were clearly identifiable on freshly prepared electrodes (Fig. 5Aii) and remained detectable after one-month operation (Fig. 5iv), frequently surrounded by additional morphotypes, including cocci and short rods likely derived from environmental colonization. These observations indicated that the initial *Bacillus* inoculum acted as stable founding population and subsequently coexisted with environmental colonizers recruited from the soil matrix. In contrast, non-functionalized control electrodes exhibited noticeably poorer bacterial adhesion, with cells sparsely distributed and restricted to exposed carbon surfaces (Fig. 5Av and 5Avi), suggesting limited spontaneous biofilm formation under identical operational conditions.

The functional performance of the anodes was further examined through metabolic activity assays using Presto blue [44], which quantified metabolic activity (and bacterial energy production capacity) through the reduction of resazurin to fluorescent resorufin. SF-PB-BS electrodes displayed markedly higher fluorescence intensities relative to unmodified carbon felt, demonstrating enhanced microbial viability

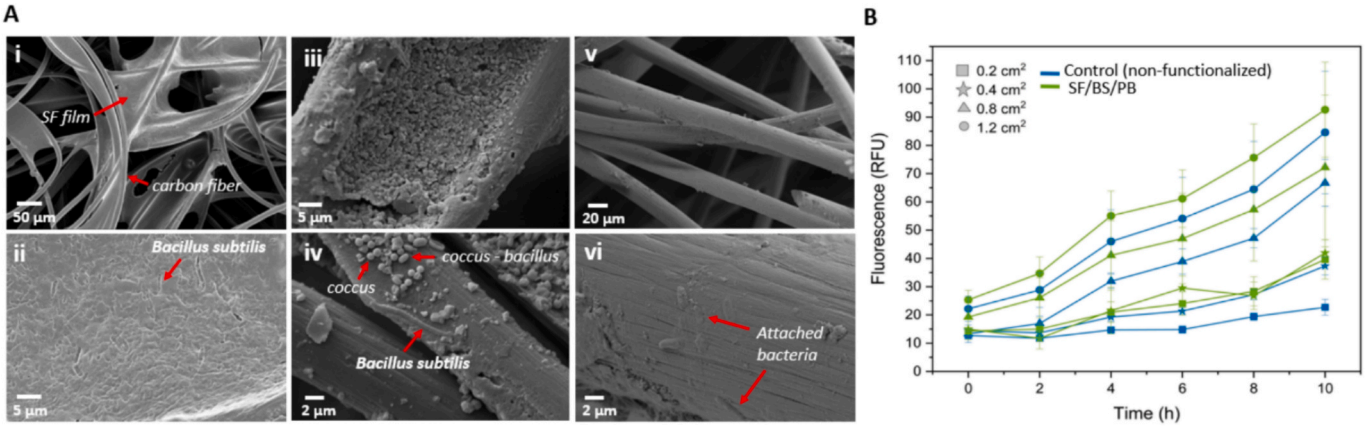

Fig. 5. SEM imaging of bioanodes and post-operational bioactivity. (A)(i and ii) Freshly functionalized SF-PB-BS bioanode showing SF membrane and immobilized *Bacillus subtilis*. (iii and iv) Same bioanode after one month in operation, showing membrane stability and extensive bacterial colonization. (v and vi) Control electrode without functionalization after one month in operation, showing limited bacterial adhesion. Scale bars represent 50, 20, 5, and 2 μm. (B) Presto blue fluorescence (RFU) over time for functionalized and control electrodes with different surface areas (0.2, 0.4, 0.8, and 1.2 cm^2), indicating higher metabolic activity in SF-PB-BS samples. Data represent mean ± standard deviation (n = 3). (For interpretation of the references to colour in this figure legend, the reader is referred to the web version of this article.)

and electron-transfer capacity (Fig. 5B). In addition, fluorescence scaled proportionally with electrode surface area, confirming the uniformity of bacterial colonization across the modified anodes. These results indicated that the synergistic combination of fibroin, *Bacillus subtilis* and Prussian blue produced a metabolically active and spatially homogeneous biofilm that support a dense, stable and electrochemically competent microbial consortium over extended operation times.

16S rRNA sequencing provide further insight into how the different electrode treatments shaped microbial community structure at the end of the operation period. Across all samples, 8,377,370 reads were recovered, predominantly classified as Bacteria (only 1.36% were classified as Archaea) and distributed in 40 phyla and 417 genera, confirming the complexity of the soil-derived inoculum.

Although community richness (Chao1 and observed taxa) did not significantly differ among electrode functionalization (Fig. S5B, Supplementary Table S1), indices of evenness and diversity (Pielou and Shannon) revealed clear modification-dependent effects. The SF-BS electrodes exhibited the highest diversity and evenness, followed by SF-PB-BS, whereas control and SF-only samples displayed comparatively less structured communities. This suggests that the presence of immobilized *Bacillus subtilis* supported a more balanced and cohesive biofilm architecture.

Beta-diversity analysis reinforced these findings. NMDS ordination revealed distinct clustering between control and functionalized electrodes, demonstrating that SF, PB and *Bacillus* played a significant role in shaping biofilm composition (Fig. 6A). Control samples clustered separately, reflexing a distinct community, less homogeneous and structured, as also indicated by the Shannon index (Fig. S5A). SF-BS and SF-PB occupied opposite regions of ordination space, indicating that the effects of *Bacillus* and PB on community assembly were independent and mechanistically distinct. SF-BS samples showed a more structured and homogeneous community (Shannon index = 4.75 ± 0.47), while SF-PB communities were more heterogeneous (Shannon index = 3.45 ± 0.19), influenced by the presence of the mediator. The SF-PB-BS electrodes positioned between these groups, consistent with the combined influence of both functionalizations.

Taxonomic analysis at the phylum (Fig. 6B) and genus level (Fig. 7) supported previous operational and functional observations. While *Desulfobacterota, Bacteroidota, Firmicutes and Proteobacteria* dominated all samples, their relative proportions varied across membrane compositions. PB-containing electrodes, particularly SF-PB, were enriched in Proteobacteria and electrogenic genera such as *Geoalkalibacter*, consistent with the mediator capacity to facilitate extracellular electron transfer and favour redox-active taxa. Electrodes containing *Bacillus* (SF-BS and SF-PB-BS) displayed higher abundances of Firmicutes, including the inoculated *Bacillus* itself, as well as genera such as *Sedimentibacter* and *Membranicola*, suggesting sustained colonization and broader community structuring by the immobilized strain.

Control electrodes, by contrast, were enriched in taxa as *Trichloromonas*, *Truepera*, *Desulfovibrio* and *Aequorivita*. In particular, *Trichloromonas* in the absence of *Bacillus* but diminished in SF-BS and SF-PB-BS functionalizations, suggesting competitive suppression by *Bacillus* or alteration of the microenvironment by the silk matrix. Previous studies have identified *Trichloromonas* as a relevant electrogene in MFCs, highlighting the specificity of the selective pressures imposed by the functionalized electrodes [45,46].

Finally, several genera associated with established exoelectrogenic activity were significantly enriched in modified electrodes. *Pseudomonas* and *Lutispora* (Fig. 7), both capable of extracellular electron transfer [47] and key contributors to nutrient cycling in soil [48], were more abundant in all modified electrodes compared to the control. PB-containing electrodes displayed particularly high levels of *Geoalkalibacter* (18%) (Fig. S6), a genus known for generating high current densities and often dominant in soil-derived microbial electrochemical systems [49,50]. The co-occurrence of these electrogenic taxa with stable membrane-supported biofilms explains the improved start-up kinetics, increased current density, and sustained performance observed in SF-PB-BS systems.

Overall, the integrated structural, metabolic and community analysis demonstrate that the SF-PB-BS modification generates a stable, diverse and electroactive biofilm strongly aligned with the enhanced electrochemical output of these bioanodes. The silk-based immobilization strategy promotes long-term physical integrity, facilitates bacterial recruitment and shapes a microbial consortium optimized for extracellular electron transfer, thereby confirming the synergistic value of combining *Bacillus* and Prussian blue within the silk matrix for high performance sMFC operation.

Conclusions

This study demonstrates that SF-based biofunctionalized anodes provide an effective, sustainable, and scalable strategy to enhance the performance of sMFCs. Immobilization of *Bacillus subtilis* within a biocompatible SF matrix preserved high bacterial viability and metabolic activity, resulting in accelerated start-up and enhanced current generation compared to unmodified carbon felt electrodes. The porous

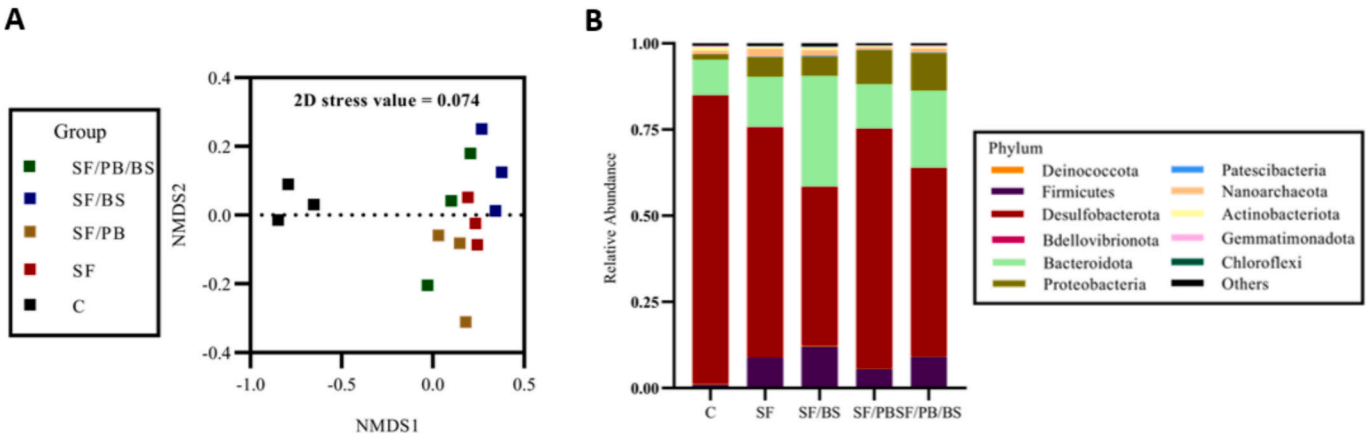

Fig. 6. Ordination analysis and relative abundance studies in bioanodes. Non-metric multidimensional scaling (NMDS) ordination based on community composition data (A). The analysis was performed using Bray–Curtis dissimilarities (2D stress = 0.074). Relative abundance of bacterial 12 most abundant phyla across different silk fibroin-based functionalizations (B). Electrode modifications include the control (C), silk fibroin (SF), silk fibroin with *Bacillus subtilis* (SF-BS), silk fibroin with Prussian blue (SF-PB), and silk fibroin with *Bacillus subtilis* and Prussian blue (SF-PB-BS). (For interpretation of the references to colour in this figure legend, the reader is referred to the web version of this article.)

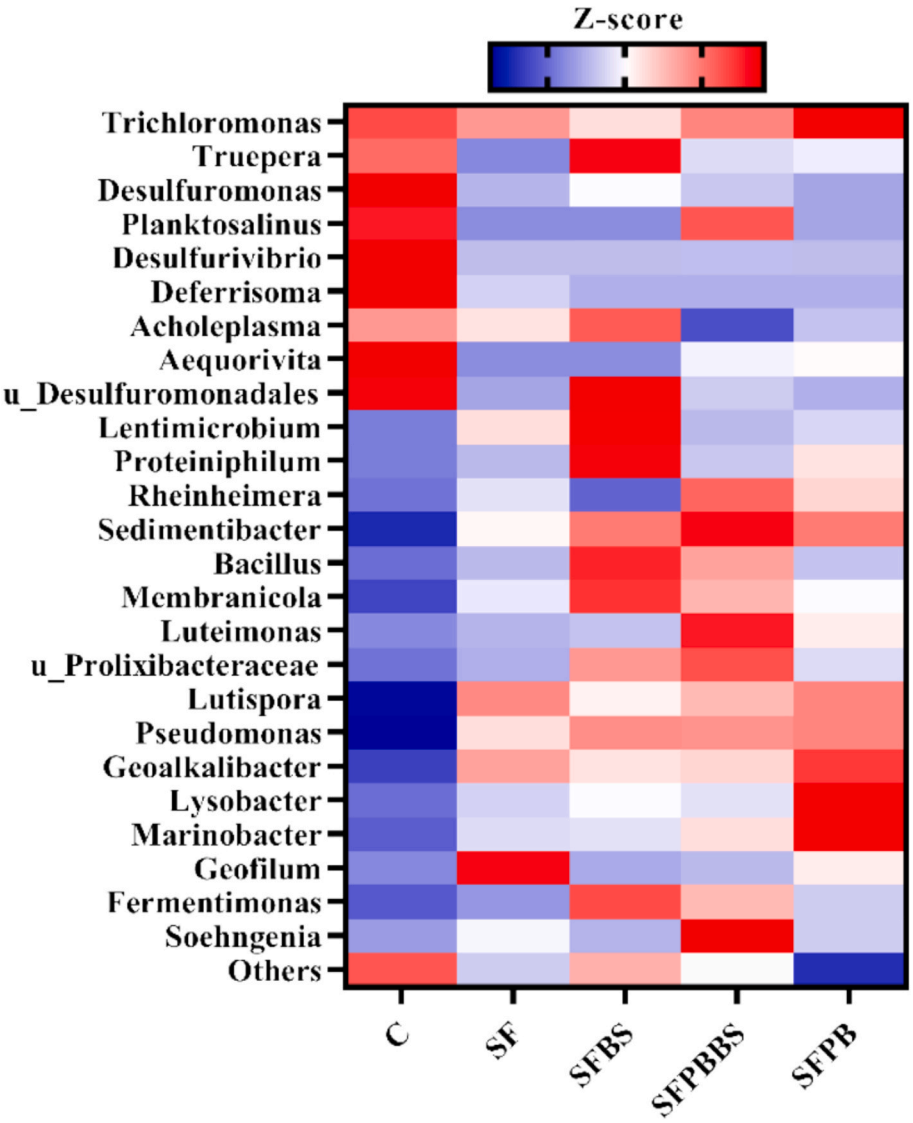

Fig. 7. Heatmap showing the relative abundance of dominant bacterial genera across treatments. The graph was created using the 15 genera that had the highest average relative abundance in each group. This resulted in a total of 26 genera. The treatments include control (C), silk fibroin (SF), silk fibroin with Prussian blue (SF/PB), silk fibroin with *Bacillus subtilis* (SF/BS), and silk fibroin with *Bacillus subtilis* and Prussian blue (SF/PB/BS). Color gradients represent standardized abundance (z-scores), with red indicating higher and blue indicating lower relative abundance. (For interpretation of the references to colour in this figure legend, the reader is referred to the web version of this article.)

and permeable structure of SF enabled efficient nutrient exchange and supported both bacterial proliferation and recruitment of additional soil-derived electrogens during operation.

The co-immobilization of PB as a redox mediator further amplified electron-transfer efficiency. PB-containing electrodes, particularly the SF-PB-BS configuration, exhibited the most pronounced improvements, including current increases of up to 68% relative to controls, a reduction in start-up time from 8 to 4 days, and superior performance during intermediate and long-term operation. Post-operational SEM imaging, metabolic assays, and 16S rRNA sequencing confirmed the formation of dense, metabolically active and selectively enriched electroactive biofilms, providing a robust biological basis for the enhanced electrochemical behaviour observed. Although the absolute power output remained in the μW range, the resulting power densities are consistent with those reported for comparable soil-based MFCs and are suitable for decentralized, low-power applications such as environmental sensors or IoT nodes.

A key outcome of this work is the development of a green, scalable and biocompatible SF crystallization protocol that enables the functionalization of large electrode areas (95 cm^2) in a single, vacuum-free drying step (5 h), without the use of toxic solvents or multi-step annealing treatments that can compromise bacterial structure or function (patent number EP25383502.9). This simplified immobilization strategy is compatible with industrial processing and supports reproducible electrode performance across different scales. Using the same strategy, electrode areas of up to approximately 655 cm^2 have been successfully tested. Beyond this size, modular interconnection of multiple sMFC units is expected to represent a more efficient and economically viable strategy for increasing overall power output than further enlargement of individual electrodes.

The immobilization strategy described here is generic and can be adapted to other bacterial strains or tailored microbial consortia, potentially enabling functionalities beyond electrogenesis, such as bioremediation or bioproduction. While the present sMFC was intentionally designed as a closed system for stable and controlled energy generation, future adaptations combining this immobilization approach with alternative reactor configurations and direct electrode-soil contact could extend its application scope. Overall, this work advances the

design of living bioelectronic interfaces and contributes to the development of sustainable, nature-inspired energy technologies for low-impact energy generation and environmental monitoring.

Ethical approval.

This study did not involve human participants or animals.

CRediT authorship contribution statement

Pablo Rodríguez-Núñez: Writing – original draft, Validation, Methodology, Investigation, Formal analysis, Data curation, Conceptualization. **Sebastián Gavira-Aguilar:** Writing – review & editing, Validation, Methodology, Investigation. **Silvia Mena:** Writing – review & editing, Validation, Methodology, Investigation. **Aida Visús:** Writing – review & editing, Validation, Methodology, Investigation, Formal analysis. **Nuria Vigués:** Writing – review & editing, Validation, Resources, Methodology, Investigation. **Jordi Mas:** Resources, Conceptualization. **Salvador D. Aznar-Cervantes:** Writing – review & editing, Resources, Investigation. **Naroa Uria:** Writing – original draft, Validation, Resources, Investigation, Funding acquisition, Data curation, Conceptualization. **Ignacio Moro:** Writing – original draft, Investigation, Data curation. **Antonio Solares:** Writing – review & editing, Validation, Methodology, Investigation, Formal analysis, Data curation. **Sara Santiago:** Writing – review & editing, Supervision, Methodology, Investigation. **Xavier Muñoz-Berbel:** Writing – review & editing, Supervision, Resources, Funding acquisition, Conceptualization.

Funding

This work was supported by the European Commission through the project SOIL2POWER (HORIZON-EIC-2022-TRANSITIONOPEN-01–101112669) and CONFETI (HORIZON-EIC-2022 PATHFINDER-CHALLENGES-01–101115182). This work was also partially funded by the MICINN – State Research Agency – AEI– (PID2021-127653NB-C21). Dr. Salvador Aznar acknowledges partial financial support from the European Commission ERDF/FEDER Operational Programme of Murcia (2021–2027), Project No. 50463.

Declaration of competing interest

The authors declare that they have no known competing financial interests or personal relationships that could have appeared to influence the work reported in this paper.

Acknowledgements

This work was supported by the European Commission through the project SOIL2POWER (HORIZON-EIC-2022-TRANSITIONOPEN-01-101112669) and CONFETI (HORIZON-EIC-2022 PATHFINDER CHALLENGES-01-101115182) and MICINN – State Research Agency – AEI– (PID2021-127653NB-C21 and PID2024-157813OB-C21). Dr. Salvador Aznar acknowledges partial financial support from the European Commission ERDF/FEDER Operational Programme of Murcia (2021-2027), Project No. 50463.

Appendix A. Supplementary data

Supplementary data to this article can be found online at https://doi.org/10.1016/j.seta.2026.104915.

Data availability

Data will be made available on request.

References

[1] Du Z, Li H, Gu T. A state of the art review on microbial fuel cells: a promising technology for wastewater treatment and bioenergy. Biotechnol Adv 2007;25:464–82. https://doi.org/10.1016/j.biotechadv.2007.05.004.
[2] Vishwanathan AS. Microbial fuel cells: a comprehensive review for beginners. 3 Biotech 2021;11(5):248. https://doi.org/10.1007/s13205-021-02802-y.
[3] Logan BE, Hamelers B, Rozendal R, Schröde U, Keller J, Freguia S, et al. Microbial fuel cells: methodology and technology. Environ Sci Technol 2006;40(17):5181–92. https://doi.org/10.1021/es0605016.
[4] Pant D, Van Bogaert G, Diels L, Vanbroekhoven K. A review of the substrates used in microbial fuel cells (MFCs) for sustainable energy production. Bioresour Technol 2010;101(6):1533–43. https://doi.org/10.1016/j.biortech.2009.10.017.
[5] Kim BH, Chang IS, Gadd GM. Challenges in microbial fuel cell development and operation. Appl Microbiol Biotechnol 2007;76(3):485–94. https://doi.org/10.1007/s00253-007-1027-4.
[6] Kwon G, Heo B, Kwon MJ, Kim I, Chu J, Kim BY, et al. Effect of silk fibroin biomaterial coating on cell viability and intestinal adhesion of probiotic bacteria. J Microbiol Biotechnol 2021;31(4):592. https://doi.org/10.4014/jmb.2103.03031.
[7] Pujol-Vila F, Dietvorst J, Gall-Mas L, Díaz-González M, Vigués N, Mas J, et al. Bioelectrochromic hydrogel for fast antibiotic-susceptibility testing. J Colloid Interface Sci 2018;511:251–8. https://doi.org/10.1016/j.jcis.2017.09.004.
[8] Vigués N, Pujol-Vila F, Marquez-Maqueda A, Muñoz-Berbel X, Mas J. Electro-addressable conductive alginate hydrogel for bacterial trapping and general toxicity determination. Anal Chim Acta 2018;1036:115–20. https://doi.org/10.1016/j.aca.2018.06.062.
[9] Forner E, Ezenarro JJ, Pérez-Montero M, Vigués N, Asensio-Grau A, Andrés A, et al. Electrochemical biosensor for aerobic acetate detection. Talanta 2023;265:124882. https://doi.org/10.1016/j.talanta.2023.124882.
[10] Cheng L, Jiang L, Yang X, et al. The performance of microbial fuel cell with sodium alginate and super activated carbon composite gel modified anode. AMB Expr 2024;14:67. https://doi.org/10.1186/s13568-024-01723-2.
[11] Alkotaini B, Tinucci SL, Robertson SJ, Hasan K, Minteer SD, Grattieri M. Alginate-Encapsulated Bacteria for the Treatment of Hypersaline Solutions in Microbial fuel Cells. Chembiochem 2018;19(11):1162–9. https://doi.org/10.1002/cbic.201800142.
[12] Wang K, Ma Q, Zhou HT, Zhao JM, Cao M, Wang SD. Review on fabrication and application of regenerated Bombyx mori silk fibroin materials. AUTEX Research Journal 2023;23(2):164–83. https://doi.org/10.2478/aut-2021-0059.
[13] Fitó-Parera A, Márquez A, Rodríguez-Núñez P, Aznar-Cervantes SD, Reguera C, Perdigones F, et al. Silkworm Gut Fibre-based Biosensors for Optical Glucose Detection. Sens Actuators Rep 2025;100378. https://doi.org/10.1016/j.snr.2025.100378.
[14] Prakash NJ, Mane PP, George SM, Kandasubramanian B. Silk fibroin as an immobilization matrix for sensing applications. ACS Biomater Sci Eng 2021;7(6):2015–42. https://doi.org/10.1021/acsbiomaterials.1c00080.
[15] Márquez A, Santiago S, Dos Santos MV, Aznar-Cervantes SD, Domínguez C, Omenetto FG, et al. Reusable colorimetric biosensors on sustainable silk-based platforms. ACS Appl Bio Mater 2024;7(2):853–62. https://doi.org/10.1021/acsabm.3c00872.
[16] Zhou W, Xie Z, Si R, Chen Z, Javeed A, Li J, et al. Actinomycin-X2-immobilized silk fibroin film with enhanced antimicrobial and wound healing activities. Int J Mol Sci 2023;24(7):6269. https://doi.org/10.3390/ijms24076269.
[17] Shimanovich U, Ruggeri FS, De Genst E, Adamcik J, Barros TP, Porter D, et al. Silk micrococoons for protein stabilisation and molecular encapsulation. Nat Commun 2017;8(1):15902. https://doi.org/10.1038/ncomms15902.
[18] Xiao M, Yao J, Shao Z, Chen X. Silk-based 3D porous scaffolds for tissue engineering. ACS Biomater Sci Eng 2024;10(5):2827–40.
[19] Yildirim S, Borer ME, Wenk E, Meinel L, Lacroix C. Development of silk fibroin-based beads for immobilized cell fermentations. J Microencapsul 2010;27(1):1–9. https://doi.org/10.3109/02652040802217516.
[20] Lv S. Silk fibroin-based materials for catalyst immobilization. Molecules 2020;25(21):4929. https://doi.org/10.3390/molecules25214929.
[21] Guan H, Ding F, Xue Y, Zhao J. Engineering the mechanical characteristics of regenerated silk fibroin materials: the impact of chemical and physical modification strategies. Front Chem 2025;13:1606995. https://doi.org/10.3389/fchem.2025.1606995.
[22] Reizabal A, Costa CM, Pérez-Álvarez L, Vilas-Vilela JL, Lanceros-Méndez S. Silk fibroin as sustainable advanced material: material properties and characteristics, processing, and applications. Adv Funct Mater 2023;33(3):2210764. https://doi.org/10.1002/adfm.202210764.
[23] Yavarinasab A, He J, Mookherjee A, Krishnan N, Pestana LR, Fusco D, et al. Electrogenic dynamics of biofilm formation: Correlation between genetic expression and electrochemical activity in *Bacillus subtilis*. Biosens Bioelectron 2025;276:117218. https://doi.org/10.1016/j.bios.2025.117218.
[24] Xu X, Pioppi A, Kiesewalter HT, Strube ML, Kovács ÁT. Disentangling the factors defining *Bacillus subtilis* group species abundance in natural soils. Environ Microbiol 2024;26(9):16693. https://doi.org/10.1111/1462-2920.16693.
[25] Estelrich J, Busquets MA. Prussian blue: a nanozyme with versatile catalytic properties. Int J Mol Sci 2021;22(11):5993. https://doi.org/10.3390/ijms22115993.
[26] Jahn MK, Haderlein SB, Meckenstock RU. Reduction of Prussian Blue by the two iron-reducing microorganisms Geobacter metallireducens and Shewanella alga. Environ Microbiol 2006;8(2):362–7. https://doi.org/10.1111/j.1462-2920.2005.00902.x.

[27] Ferrer-Vilanova A, Alonso Y, J Ezenarro J, Santiago S, Muñoz-Berbel X, Guirado G. Electrochromogenic detection of live bacteria using soluble and insoluble Prussian blue. ACS omega 2021;6(46):30989-30997. Doi: 10.1021/acsomega.1c03434.
[28] Ferrer-Vilanova A, Ezenarro JJ, Ivanova K, Calvo Ó, Perelshtein I, Gorni G, et al. Smart bactericidal textile enabling in-situ visual assessment of antimicrobial activity. Mater Today Bio 2025;32:101724. https://doi.org/10.1016/j.mtbio.2025.101724.
[29] Ferrer-Vilanova A, Alonso Y, Dietvorst J, Pérez-Montero M, Rodríguez-Rodríguez R, Ivanova K, et al. Sonochemical coating of Prussian Blue for the production of smart bacterial-sensing hospital textiles. Ultrason Sonochem 2021;70:105317. https://doi.org/10.1016/j.ultsonch.2020.105317.
[30] Uría N, Muñoz Berbel X, Sánchez O, Muñoz FX, Mas J. Transient storage of electrical charge in biofilms of Shewanella oneidensis MR-1 growing in a microbial fuel cell. Environ Sci Technol 2011;45(23):10250–6. https://doi.org/10.1021/es2025214.
[31] Abouhagger A, Celiešiūtė-Germanienė R, Bakute N, Stirke A, Melo WC. Electrochemical biosensors on microfluidic chips as promising tools to study microbial biofilms: a review. Front Cell Infect Microbiol 2024;14:1419570. https://doi.org/10.3389/fcimb.2024.1419570.
[32] "Differential Pulse Voltammetry." ScienceDirect Topics, Elsevier, https://www.sciencedirect.com/topics/chemistry/differential-pulse-voltammetry. Accessed 28 Feb. 2024.
[33] Chen S, Tang J, Fu L, Yuan Y, Zhou S. Biochar improves sediment microbial fuel cell performance in low conductivity freshwater sediment. Journal of Soils and Sediments 20160;16(9):2326-2334. Doi: 10.1007/s11368-016-1452-z.
[34] Magoč T, Salzberg SL. FLASH: fast length adjustment of short reads to improve genome assemblies. Bioinformatics 2011;27(21):2957–63. https://doi.org/10.1093/bioinformatics/btr507.
[35] Bokulich NA, Subramanian S, Faith JJ, Gevers D, Gordon JI, Knight R, et al. Quality-filtering vastly improves diversity estimates from Illumina amplicon sequencing. Nat Methods 2013;10(1):57–9. https://doi.org/10.1038/nmeth.2276.
[36] Oksanen J, Blanchet FG, Friendly M, Kindt R, Legendre P, McGlinn D, et al. Vegan: Community Ecology Package 2022. R package version 2.6-4. https://CRAN.R-project.org/package=vegan.
[37] R Core Team. R: A language and environment for statistical computing. R Foundation for Statistical Computing 2022. Vienna, Austria. https://www.R-project.org/.
[38] Härtig E, Jahn D. Regulation of the anaerobic metabolism in *Bacillus subtilis*. Adv Microb Physiol 2012;61:195–216. https://doi.org/10.1016/b978-0-12-394423-8.00005-6.
[39] Amirikia M, Shariatzadeh SMA, Jorsaraei SGA, Mehranjani MS. Auto fluorescence of a silk fibroin-based scaffold and its interference with fluorophores in labeled cells. Eur Biophys J 2018;47(5):573–81. https://doi.org/10.1007/s00249-018-1279-1.
[40] Dziegielowski J, Mascia M, Metcalfe B, Di Lorenzo M. Voltage evolution and electrochemical behaviour of Soil microbial fuel cells operated in different quality soils. Sustainable Energy Technol Assess 2023;56:103071. https://doi.org/10.1016/j.seta.2023.103071.
[41] Dongre A, Sharma RK, Sogani M, Poddar NK. Ultrasonic pre-treatment of bacillus velezensis for improved electrogenic response in a single chambered microbial fuel cell. 3 Biotech 2022;12(1):18. https://doi.org/10.1007/s13205-021-03065-3.
[42] Xu L, Zhang G, Chen J, Fu L, Yang F. Prussian blue/graphene-modified electrode used as a novel oxygen reduction cathode in microbial fuel cell. J Taiwan Inst Chem Eng 2016;58:374–80. https://doi.org/10.1016/j.jtice.2015.06.013.
[43] Yen B, Jaliff L, Gutierrez L, Sahinidis P, Bernstein S, Madden J, et al. Soil-powered computing: the engineer's guide to practical soil microbial fuel cell design. Proc ACM Interact Mobile Wearable Ubiquitous Technol 2024;7(4):1–40. https://doi.org/10.1145/363141.
[44] Braissant O, Astasov-Frauenhoffer M, Waltimo T, Bonkat G. A review of methods to determine viability, vitality, and metabolic rates in microbiology. Front Microbiol 2020;11:547458. https://doi.org/10.3389/fmicb.2020.547458.
[45] Jangir Y, Guo Y, Connon S, Pontrelli S, Wu F, Schwartzman J, et al. Deep sea anaerobic microbial community couples the degradation of insoluble chitin to extracellular electron transfer. BioRxiv 2025. https://doi.org/10.1101/2025.06.30.662270.
[46] Lascu I, Locovei C, Bradu C, Gheorghiu C, Tanase AM, Dumitru A. Polyaniline-derived nitrogen-containing carbon nanostructures with different morphologies as anode modifier in microbial fuel cells. Int J Mol Sci 2022;23(19):11230. https://doi.org/10.3390/ijms231911230.
[47] Li P, Yuan W, Huang Y, Zhang C, Ni C, Lin Q, et al. Complete genome sequence of *Pseudomonas stutzeri* S116 owning bifunctional catalysis provides insights into affecting performance of microbial fuel cells. BMC Microbiol 2022;22(1):137. https://doi.org/10.1186/s12866-022-02552-8.
[48] Rabiço F, Pedrino M, Narcizo JP, de Andrade AR, Reginatto V, Guazzaroni ME. Synthetic Biology Toolkit for a New Species of Pseudomonas Promissory for Electricity Generation in Microbial fuel Cells. Microorganisms 2023;11(8):2044. https://doi.org/10.3390/microorganisms11082044.
[49] Badalamenti JP, Krajmalnik-Brown R, Torres CI. Generation of high current densities by pure cultures of anode-respiring Geoalkalibacter spp. under alkaline and saline conditions in microbial electrochemical cells. MBio 2103;4(3):10-1128. Doi: 10.1128/mBio.00144-13.
[50] Hamdan HZ, Salam DA. Ferric iron stimulation in marine SMFCs: impact on the microbial structure evolution in contaminated sediments with low and high molecular weight PAHs. J Environ Manage 2021;280:111636. https://doi.org/10.1016/j.jenvman.2020.111636.